

ON THE VIABILITY OF THE MAGNETOROTATIONAL INSTABILITY IN CIRCUMPLANETARY DISKS

YURI I. FUJII¹, SATOSHI OKUZUMI^{1,2}, TAKAYUKI TANIGAWA³, AND SHU-ICHIRO INUTSUKA¹

Draft version March 23, 2018

ABSTRACT

We examine whether the magnetorotational instability (MRI) can serve as a mechanism of angular momentum transport in circumplanetary disks. For the MRI to operate the ionization degree must be sufficiently high and the magnetic pressure must be sufficiently lower than the gas pressure. We calculate the spatial distribution of the ionization degree and search for the MRI-active region where the two criteria are met. We find that there can be thin active layers at the disk surface depending on the model parameters, however, we find hardly any region which can sustain well-developed MRI turbulence; when the magnetic field is enhanced by MRI turbulence at the disk surface layer, a magnetically dominated atmosphere encroaches on a lower altitude and a region of well-developed MRI turbulence becomes smaller. We conclude that if there are no angular momentum transfer mechanisms other than MRI in gravitationally stable circumplanetary disks, gas is likely to pile up until disks become gravitationally unstable, and massive disks may survive for a long time.

Subject headings: dust, extinction – planets and satellites: formation – protoplanetary disks

1. INTRODUCTION

Gas giant planets obtain mass from surrounding protoplanetary disks during their formation. When gas flows onto the planets, disks form around them as by-products. These gaseous disks are called circumplanetary disks. The evolution of circumplanetary disks is important not only for the formation of gas giants but also for the formation of satellites because regular satellites are thought to form in circumplanetary disks. There have been several theoretical studies of satellite formation in disks (e.g., Lunine & Stevenson 1982; Canup & Ward 2002, 2006; Mosqueira & Estrada 2003a,b; Canup & Ward 2009; Estrada et al. 2009; Sasaki et al. 2010; Ogihara & Ida 2012). Canup & Ward (2002, 2006) developed a so-called gas-starved disk model and successfully explained the total mass of the Galilean satellites and other satellite systems around giant planets in our solar system. In their scenario, gas and solids are continuously supplied to circumplanetary disks and satellites form and migrate onto the central planet repeatedly; the last generation of satellites remains when the mass inflow terminates. Mosqueira & Estrada (2003a,b) developed a so-called solid enhanced minimum mass disk model and reproduced the Galilean satellites; the inner three satellites are formed in an inner massive disk and the outermost satellite is formed slowly in an outer extended low-density disk. A remaining problem is how to form circumplanetary disks accounting for their viscous evolution and mass infall from protoplanetary disks. Recently, a new idea for satellite formation has been advocated by Crida & Charnoz (2012). Using their gas-free tidal-spreading particle disk model, the mass distributions of most regular satellite systems in our solar system can be well reproduced. However, it is difficult to form Galilean satellites in this model, which would imply that the satellites still need a gaseous circumplanetary disk for their formation.

Hydrodynamic simulations of gas giant formation (e.g., Lubow et al. 1999; Tanigawa & Watanabe 2002; Ayliffe & Bate 2009b,a; Machida et al. 2006, 2008, 2010) have shown that circumplanetary disks form during the accretion phases of giant planets. Since most of these studies focused on gas giant formation, the detailed distribution of gas flow onto a circumplanetary disk was not well investigated. Recently, high-resolution 3D simulations by Tanigawa et al. (2012) have demonstrated that gas flows onto circumplanetary disks from high altitudes, not from the disk mid-plane. This was the first detailed analysis of the flux of gas infall from protoplanetary to circumplanetary disks. This picture is consistent with radiative hydrodynamical simulations by Klahr & Kley (2006) and the very recent high-resolution global simulations by Gressel et al. (2013) and Szulagyi et al. (2014).

On the other hand, the driving mechanism of angular momentum transfer of gas in circumplanetary disks is not yet well understood. For accretion disks in general, the most promising mechanism is believed to be the magnetic turbulence driven by the magnetorotational instability (MRI). To be MRI-active, gas in a disk should be sufficiently ionized to couple with the magnetic field. The main ionization source in circumplanetary disks is galactic cosmic rays, and their attenuating length is about 100 g cm^{-2} . In some studies of MRI, a critical surface column density of $\Sigma_{\text{crit}} \sim 100 \text{ g cm}^{-2}$ was adopted; a surface density below this value implies that the MRI can operate (Gammie 1996). However, if we take into account the chemical reactions of charged particles, such as recombination or capture by dust grains, the critical value can be far smaller (Sano, Miyama, Umebayashi, & Nakano 2000; Ilgner & Nelson 2006; Okuzumi 2009; Fujii, Okuzumi, & Inutsuka 2011). In the context of circumplanetary disks, Martin & Lubow (2011a) and Lubow & Martin (2012) pointed out the possibility of accretion outbursts induced by a combination of MRI and gravitational instability (GI).

In this work, we develop a model for circumplanetary disks by calculating the surface density with the mass infall

yuri.f@nagoya-u.jp

¹ Department of Physics, Nagoya University, Furo-cho, Chikusa-ku, Nagoya, Aichi 464-8602, Japan

² Department of Earth and Planetary Sciences, Tokyo Institute of Technology, Meguro-ku, Tokyo, 152-8551, Japan

³ Institute of Low Temperature Science, Hokkaido University, Sapporo, 060-0819, Japan

rate obtained by Tanigawa et al. (2012), and investigate whether the MRI is important in circumplanetary disks. Since Tanigawa et al. (2012) have found that the mass infall rate is proportional to the surface density of the parental protoplanetary disk, we can model the various evolution phases of the disk. We introduce a gas depletion factor and model the situation when a gas giant opens a gap, or gas in the protoplanetary disk is globally depleted. For the evaluation of MRI activity, we use the Elsasser number. The Elsasser number is proportional to the ionization degree, which we calculate for several conditions using the method developed by Fujii, Okuzumi, & Inutsuka (2011). For ionization sources, we take into account galactic cosmic rays, X-rays from the host star, and the decay of short-lived radionuclides.

In Section 2, we explain how to estimate the border of MRI-active/inactive regions in gaseous disks such as circumplanetary disks or protoplanetary disks. Our models of circumplanetary disks are described in Section 3. In Section 4, we investigate MRI activity in circumplanetary disks using our ionization degree calculation method described in Section 2. A discussion of our results is given in Section 5, and we summarize this paper in Section 6.

2. MRI AND IONIZATION DEGREE

2.1. Conditions for MRI growth

There are two criteria for the MRI to be active (Balbus & Hawley 1991; Sano & Miyama 1999; Okuzumi & Hirose 2011). First, the ionization degree of the disk gas should be high enough to couple to the magnetic field. We use the Elsasser number to investigate MRI activity. The Elsasser number is written as

$$\Lambda = \frac{v_{Az}^2}{\eta\Omega_K}, \quad (1)$$

where v_{Az} is the z component of the Alfvén velocity, η is the magnetic diffusivity, and Ω_K is the Keplerian frequency. In order for the MRI to operate, Λ must be larger than unity (Sano & Miyama 1999). The region where $\Lambda < 1$ is a dead zone. The magnetic diffusivity can be written as follows (Blaes & Balbus 1994):

$$\eta = 234 \left(\frac{T}{1\text{K}} \right)^{1/2} x_e^{-1} \text{ cm}^2 \text{ s}^{-1}, \quad (2)$$

where $x_e \equiv n_e/n_n$ (the ratio of the number densities of electrons and neutral gas molecules) is the ionization degree. Equations (1) and (2) show that Λ is proportional to the ionization degree, x_e . Here, we consider only Ohmic dissipation and neglect the ambipolar and Hall diffusivities that mostly work to stabilize the MRI. If we know the strength of the magnetic field and the temperature of the gas, we only need the ionization degree to estimate Λ (note that ions and charged dust grains are much heavier than electrons and therefore their motion is negligible). In this work, we treat the magnetic field as a parameter and calculate the ionization degree of an isothermal disk. The ratio of gas pressure, P_{gas} , and the z component of magnetic pressure, $P_{\text{mag},z}$, represents the z component of the plasma beta, which is

$$\beta_z \equiv \frac{P_{\text{gas}}}{P_{\text{mag},z}} = \frac{\rho_g c_s^2}{B_z^2/8\pi} = \frac{2c_s^2}{v_{Az}^2}, \quad (3)$$

where B_z is the net vertical magnetic field, $v_{Az} = B_z/\sqrt{4\pi\rho_g}$ is the z component of Alfvén velocity, c_s is the sound speed, which is assumed constant, and ρ_g is the gas density. Note that β_z is defined in terms of *net* magnetic flux. In this study, we assume that the disk is vertically hydrostatic (see Equation (19)) and that B_z is vertically constant. Thus, we write β_z as $\beta_0 \exp(z^2/2H^2)$, where β_0 is the mid-plane value of β_z , z is the height from the mid-plane, and H is the scale height of the disk. We assume β_0 is constant and choose $\beta_0 = 10^4$ and 10^5 , which are optimistic values for MRI. The higher net field strength means that more magnetic flux threads the disk.

Second, the wavelength of the most unstable mode, $\lambda_{\text{MRI}} = 2\pi v_A/\Omega_K$, should be smaller than the scale height of the disk. This corresponds to the condition for a weak magnetic field: if the magnetic field is too strong, magnetic tension prevents disk gas from becoming turbulent. We refer to the region with $\lambda_{\text{MRI}} > H$ as the magnetically dominated atmosphere where the MRI is suppressed. Thus, from Equation (3), the condition to be MRI-active is written as

$$2\pi v_A/\Omega_K = \lambda_{\text{MRI}} < H = c_s/\Omega_K, \quad (4)$$

or equivalently,

$$\beta_z > 8\pi^2. \quad (5)$$

When the MRI is driven, magnetic fields are amplified by turbulence and the magnetically dominated atmosphere encroaches on the active region. Okuzumi & Ormel (2013) quantitatively evaluated this using MHD simulations by Okuzumi & Hirose (2011) and Gressel et al. (2012). At the border separating active from dead zones, B_z^2 is amplified to be roughly 30 times larger than the original value. (see Equation (37) of Okuzumi & Ormel 2013). This implies that the real plasma beta at the border becomes $\beta_z/30$. Thus, when the turbulence is well-developed, the criterion to have MRI becomes $\beta_z/30 > 8\pi^2$, or approximately,

$$\beta_z \gtrsim 2000. \quad (6)$$

The lower limit of the magnetically dominated atmosphere is located between $1.8H$ and $3.8H$, depending on β_0 and the criteria of the second condition (see Figs. 3, 4, and 5). We ignore the effect of mixing on chemistry because it is important only above about $3H$, or even higher when there are dust grains. The onset of the MRI occurs only in the region where the two conditions of Equation (1) and (5) are both met. The conditions to have well-developed MRI turbulence are severer than those of just onset of the MRI, which are Equation (1) and (6).

2.2. Calculation of ionization degree

We calculate the ionization degree accounting for dust grains. We assume that there are plentiful metal ions so that molecular ions transfer their charge to metal ions quickly. We use the following rate equations derived by Fujii, Okuzumi, & Inutsuka (2011) based on Oppenheimer & Dalgarno (1974) and Okuzumi (2009):

$$\frac{dn_{M^+}}{dt} = \zeta n_n - \alpha_{M^+} n_{M^+} n_e - \langle k_{M^+d} \rangle N_d n_{M^+}, \quad (7)$$

$$\frac{dn_e}{dt} = \zeta n_n - \alpha_{M^+} n_{M^+} n_e - \langle k_{ed} \rangle N_d n_e, \quad (8)$$

$$\frac{d\langle Z \rangle}{dt} = \langle k_{M^+d} \rangle n_{M^+} - \langle k_{ed} \rangle n_e, \quad (9)$$

$$\begin{aligned} \frac{d\langle \delta Z^2 \rangle}{dt} = & (\langle k_{M^+d} \rangle + 2\langle k_{M^+d} \delta Z \rangle) n_{M^+} \\ & + (\langle k_{ed} \rangle - 2\langle k_{ed} \delta Z \rangle) n_e. \end{aligned} \quad (10)$$

where n_j indicates the number density of each particles (n, neutral molecules; e, electrons; M^+ , metal ions), N_d , $\langle Z \rangle$, and $\langle \delta Z^2 \rangle$ are the total number density, mean charge, and dispersion of the charge distribution of dust grains, respectively, ζ is the ionization rate, α_{M^+} is the reaction rate of radiative recombination, and $\langle k_{jd} \rangle$ is the capture rate onto a dust grain surface weighted by the number density of dust grains of charge Z . We use the UMIST database (RATE'06) for $\alpha_{M^+} = 2.80 \times 10^{-12} (T/300 \text{ K})^{-0.86} \text{ cm}^3 \text{ s}^{-1}$, where T is temperature. In this work, we assume compact spherical dust grains with density $\rho_{\text{grain}} = 3 \text{ g cm}^{-3}$ and radii $a = 0.1$ and $10 \mu\text{m}$. The mass of a grain is $m_{\text{grain}} = (4\pi/3)\rho_{\text{grain}}a^3$. We define the dust-to-gas mass ratio as the ratio of spatial density of dust grains, ρ_d , to that of gas, ρ_g :

$$f_{\text{dg}} \equiv \frac{\rho_d}{\rho_g}, \quad (11)$$

and use $f_{\text{dg}} = 10^{-2}$. We can write the number density of dust grains as $n_d = \rho_d/m_{\text{grain}} = f_{\text{dg}}\rho_g/m_{\text{grain}}$.

2.3. Ionization rate

There are several sources of primary ionization such as galactic cosmic rays, UV and X-rays from the host star, heat caused by stellar radiation or disk viscosity, and the decay of short-lived radionuclides. Here we take into account cosmic rays, X-rays, and radionuclides as ionization sources. If we denote the radius of a disk as r and the height from the disk mid-plane as z , the ionization rate can be written as

$$\zeta(r, z) = \zeta_C + \zeta_X + \zeta_R, \quad (12)$$

where ζ_C , ζ_X , and ζ_R are the ionization rates of cosmic rays, X-rays, and radionuclides respectively. ζ_C can be calculated from the following equation (Umebayashi & Nakano 1981):

$$\zeta_C = \frac{\zeta_{\text{CR}}}{2} \left\{ \exp \left[-\frac{\chi(r, z)}{\chi_{\text{CR}}} \right] + \exp \left[-\frac{\Sigma(r) - \chi(r, z)}{\chi_{\text{CR}}} \right] \right\}, \quad (13)$$

where $\zeta_{\text{CR}} = 1.0 \times 10^{-17} \text{ s}^{-1}$ is the cosmic ray ionization rate in interstellar space. Cosmic rays may be blown out by stellar winds and the ionization rate may be lower by several orders of magnitude depending on stellar activity (Cleeves et al. 2013). $\chi_{\text{CR}} = 96 \text{ g cm}^{-2}$ is the attenuating length of cosmic rays, and $\Sigma(r)$ is the surface density of a disk at radius r , and

$$\chi(r, z) = \int_z^\infty \rho_g(r, z) dz \quad (14)$$

is the column density from z to the outside of the disk. The rate of X-ray ionization is

$$\zeta_X = \zeta_{\text{XR}} \left(\frac{r_*}{1\text{AU}} \right)^{-2} \left(\frac{L_{\text{XR}}}{2 \times 10^{30} \text{ erg s}^{-1}} \right) \left\{ \exp \left[-\frac{\chi(r, z)}{\chi_{\text{XR}}} \right] + \exp \left[-\frac{\Sigma(r) - \chi(r, z)}{\chi_{\text{XR}}} \right] \right\}, \quad (15)$$

where r_* is the distance from the host star, $L_{\text{XR}} = 2 \times 10^{30} \text{ erg s}^{-1}$ is the X-ray luminosity, and $\zeta_{\text{XR}} = 2.6 \times 10^{-15} \text{ s}^{-1}$ and $\chi_{\text{XR}} = 8.0 \text{ g cm}^{-2}$ are fitting parameters (Igea & Glassgold 1999; Turner & Sano 2008). Equation (15) only takes into account X-rays scattered by diffuse gas well above the mid-plane and neglects direct X-ray irradiation (see

Turner & Sano 2008). We use this formula since a protoplanetary disk likely blocks direct irradiation and prevents it from reaching a geometrically much thinner circumplanetary disk. A new study on X-ray ionization rates done by Ercolano & Glassgold (2013) confirmed the calculation of Igea & Glassgold (1999) and also calculated ionization rates using parameters based on current observations. The ionization rate of the decay of radionuclides is $\zeta_{\text{R}} = 7.6 \times 10^{-19} f_{\text{g}} \text{ s}^{-1}$ where f_{g} is the depletion factor of dust grains from interstellar abundance (Umebayashi & Nakano 2009). A plot of each ionization source is provided in Fig. 1.

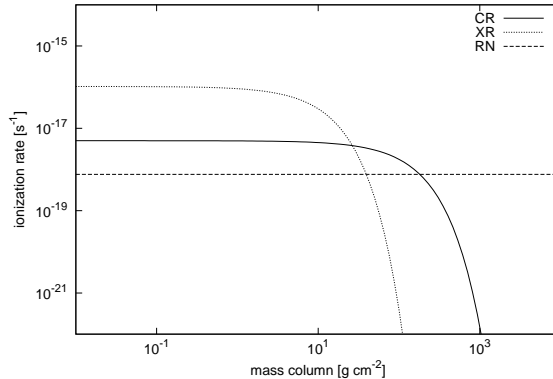


Figure 1. Ionization rates due to cosmic rays (solid line), X-rays (dotted line), and radionuclides (dashed line) as a function of the vertical mass column density χ .

If the density is high around the border of an MRI-active region and a dead zone, the main ionization source is cosmic rays and other sources are less effective at the orbit of gas giants. Large uncertainties exist about how many radionuclides are in circumplanetary disks and also how the effectiveness of X-ray ionization depends on the geometry of circumplanetary and protoplanetary disks. However, here we include X-rays and radionuclides as well as cosmic rays to obtain a maximum estimate of ionization degree.

3. DISK MODEL

3.1. Surface density of circumplanetary disks

We solve a diffusion equation for a disk with mass infall from outside the disk assuming accretion stress α (Shakura & Sunyaev 1973) and determine the surface density of the disk. The diffusion equation of surface density Σ in a Keplerian disk with a source term f is

$$\frac{\partial \Sigma}{\partial t} = \frac{1}{r} \frac{\partial}{\partial r} \left[3r^{1/2} \frac{\partial}{\partial r} \left(r^{1/2} \nu \Sigma \right) \right] + f, \quad (16)$$

where r is radius and ν is the kinematic viscosity coefficient. For f , we use the result of Tanigawa et al. (2012). They measured the physical properties of infalling gas just before it falls onto a circumplanetary disk. Since the infall is supersonic, its properties do not depend on the structure of the circumplanetary disk located at the downstream and thus the physical properties are less uncertain. They found that the mass flux and specific angular momentum of infalling gas are proportional to r^0 and r^1 , respectively. The angular momentum at the radius where gas falls onto the circumplanetary disk is smaller than that of Keplerian rotation and the radial dependence of angular momentum of infalling gas is larger than the Keplerian profile: gas will move inwards until it rotates at the Keplerian velocity if it conserves specific angular momentum, and the mass distribution becomes centrally concentrated. As a result, the effective mass flux can be approximated as $f \propto r^{-1}$. We assume that a central planet is located at an orbit of 5.2AU in a protoplanetary disk around a solar mass star. If we adopt the minimum mass solar nebula model (Hayashi 1981), the surface density and sound speed of the protoplanetary disk at 5.2AU are $\Sigma_{\text{P}} = 143 \text{ g cm}^{-2}$ and $c_{\text{sP}} = 6.58 \times 10^4 \text{ cm s}^{-1}$. We assume the central planet has a mass of 0.4 Jupiter masses. Using these values, we obtain a mass infall rate of

$$f = 1.3 \times 10^{-3} \epsilon \left(\frac{\Sigma_{\text{P}}}{143 \text{ g cm}^{-2}} \right) \left(\frac{r}{R_{\text{J}}} \right)^{-1} \text{ g cm}^{-2} \text{ s}^{-1}, \quad (17)$$

where ϵ is a depletion factor of protoplanetary disk gas, and R_{J} is the Jupiter radius. We use this formula only within $r = 20R_{\text{J}}$ and set $f = 0$ at larger radii, because the power law index of the mass infall rate drops outside $\sim 20R_{\text{J}}$ (Tanigawa et al. 2012). The parameter ϵ represents the situation when a (proto-) planet grows to some extent, and a gap opens in the disk. Since the viscous timescale of a circumplanetary disk is sufficiently smaller than that of a protoplanetary disk, we can treat ϵ as a constant. Smaller values of ϵ represent later times, and $\epsilon = 1$ corresponds to the onset of accretion. We employ the standard α prescription,

$$\nu = \alpha c_{\text{s}} H = \alpha \frac{c_{\text{s}}^2}{\Omega_{\text{K}}}. \quad (18)$$

We choose ν such that $\alpha = 0.05$.

We solve Equation (16) numerically with the initial condition $\Sigma(t = 0) = 0$, time step $\Delta t = 1.0 \times 10^3$ s, and cell width $\Delta r = 0.85R_J$. The calculation range is $0.85R_J \leq r \leq 210R_J$. The boundary conditions are that the torque vanishes at the center and at the outer boundary.

We assume that the disk is vertically hydrostatic and use the gas density profile

$$\rho_g(r, z) \equiv \frac{\Sigma}{\sqrt{2\pi}H} \exp\left(-\frac{z^2}{2H^2}\right), \quad (19)$$

and use $T = 123\text{K}$ as the temperature of the disk gas.

In Fig. 2 we plot the surface density of steady states with $\epsilon = 1, 0.1, 10^{-3},$ and 10^{-5} . Note that the critical surface density to be gravitationally unstable is several orders of magnitude larger than the case of $\epsilon = 1$.

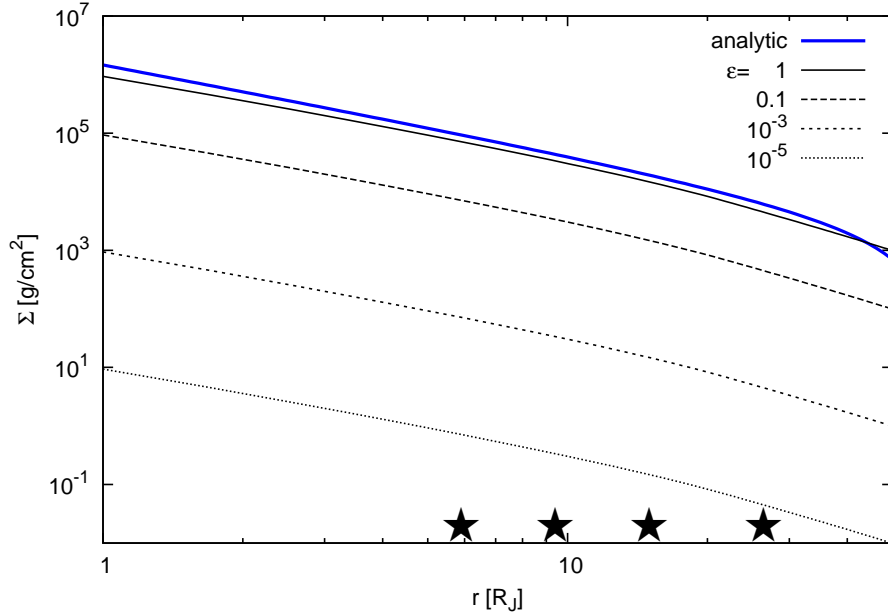


Figure 2. Surface densities of circumplanetary disks with $\alpha = 0.05$. Each line shows a different value of ϵ , the depletion factor of protoplanetary disk gas. The blue thick line is an analytic solution (see 3.2). Stars denote the orbit of Galilean satellites around Jupiter.

3.2. Analytic solution for surface density

We can analytically solve Equation (16) using Equation (18) when α is a constant value and the disk is steady and isothermal (cf. Appendix of Canup & Ward 2002). The source term f is proportional to r^{-1} so we write $f \equiv A/r$, where A is a constant. If we write $\nu = \nu_0 (r/r_0)^{\frac{3}{2}}$, where ν_0 is the kinematic viscosity coefficient for $r = r_0$, the solution of

$$0 = \frac{1}{r} \frac{\partial}{\partial r} \left[3r^{\frac{1}{2}} \frac{\partial}{\partial r} \left(r^{\frac{1}{2}} \nu \Sigma \right) \right] + \frac{A}{r}, \quad (20)$$

is

$$\Sigma = \frac{r_0^{\frac{3}{2}}}{\nu_0} \left(-\frac{2}{9} A r^{-\frac{1}{2}} + C_1 r^{-\frac{3}{2}} + C_2 r^{-2} \right), \quad (21)$$

where C_1 and C_2 are constants. C_2 should be zero since the torque $r^{1/2} \nu \Sigma$ vanishes at $r = 0$. The mass accretion rate of a steady state at the inner boundary, \dot{M}_p , is

$$\begin{aligned} \dot{M}_p &\simeq -2\pi r_{\text{in}} \Sigma v_r \\ &= 6\pi r_{\text{in}}^{\frac{1}{2}} \frac{\partial}{\partial r} \left(r_{\text{in}}^{\frac{1}{2}} \nu \Sigma \right) \\ &= 3\pi C_1, \end{aligned} \quad (22)$$

where r_{in} is the radius of the inner boundary and v_r is the radial velocity of gas. We consider the second term on the right hand side of Equation (21) to be dominant. Since the inner edge of a disk is far smaller than the outer edge of

the region with infall, r_b , the total infall rate onto the circumplanetary disk \dot{M}_s can be approximated as

$$\begin{aligned}\dot{M}_s &= 2\pi \int_{r_{\text{in}}}^{r_b} f r \, dr \\ &\simeq 2\pi A r_b.\end{aligned}\tag{23}$$

In a steady state, the mass falling onto the central planet should be equal to the inflow from the surrounding proto-planetary disk, thus $\dot{M}_p = \dot{M}_s$ and C_1 can be derived as

$$C_1 = \frac{2}{3} A r_b.\tag{24}$$

In this way, we obtain the analytic solution for the surface density:

$$\Sigma = \frac{A}{\nu_0} r_0^{\frac{3}{2}} \left(-\frac{2}{9} r^{-\frac{1}{2}} + \frac{2}{3} r_b r^{-\frac{3}{2}} \right).\tag{25}$$

This solution for $\epsilon = 1$ and $r_b = 20R_J$ is plotted in Fig. 2. We consider only the mass accreted onto the central planet and neglect the mass extending outwards, thus the analytic solution is slightly larger than the numerical solution. About 10% of the infalling mass flux exits the disk outwards.

4. IONIZATION DEGREE AND MRI-ACTIVITY IN CIRCUMPLANETARY DISKS

We calculate the ionization degree in circumplanetary disks for the surface densities obtained in Section 3. The parameters employed in our calculations are shown in Table 1. Note that cases with larger f_{dg} or smaller a than the ranges shown result in smaller MRI-active regions and the results with smaller f_{dg} or larger a approach those of the dust-free calculations. Since the magnetic field strength is uncertain, we choose optimistic values of β_0 . If we focus only on the MRI, there are no heating sources if the disk is MRI-dead. The radial profiles of temperature structure do not dramatically affect MRI-activity as long as the disk is not hot enough for thermal ionization to be effective. Thus, we assume isothermality in our calculations of ionization degree to be consistent with the earlier sections of this paper.

Table 1
Calculations parameters

parameter	value
gas depletion factor ϵ	1, 10^{-3} , 10^{-5}
dust-to-gas ratio f_{dg}	0 (dust-free), 0.01
dust radius $a[\mu\text{m}]$	0.1, 10
mid-plane value of plasma beta (z component) β_0	10^4 , 10^5

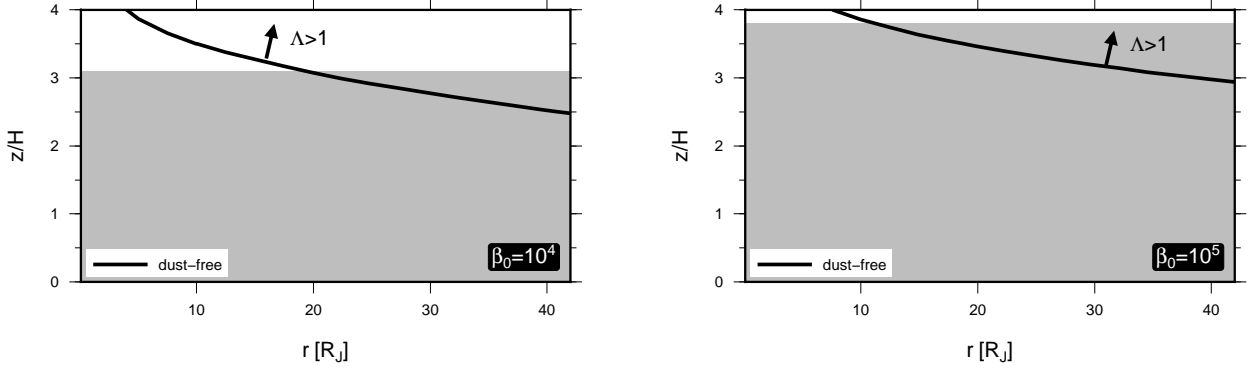


Figure 3. Borders of MRI-active/inactive regions. The horizontal axis is radius normalized by Jupiter radius, and the vertical axis is the vertical extent of the disk normalized by disk scale height. The solid lines show $\Lambda = 1$ for the dust-free case, and the region above the lines are $\Lambda > 1$. Shaded and hatched areas are the regions $\beta_z > 8\pi^2$ and $\beta_z > 2000$, respectively. The left panel is the case with $\beta_0 = 10^4$ and the right panel is the case with $\beta_0 = 10^5$. These are cases in which the infall rate is not decreased ($\epsilon = 1$). We plot only the results of dust-free cases. If there are dust grains, the ionization degree is smaller and the line $\Lambda = 1$ is higher. Gas from the protoplanetary disk infalls onto the region $r < 20 R_J$.

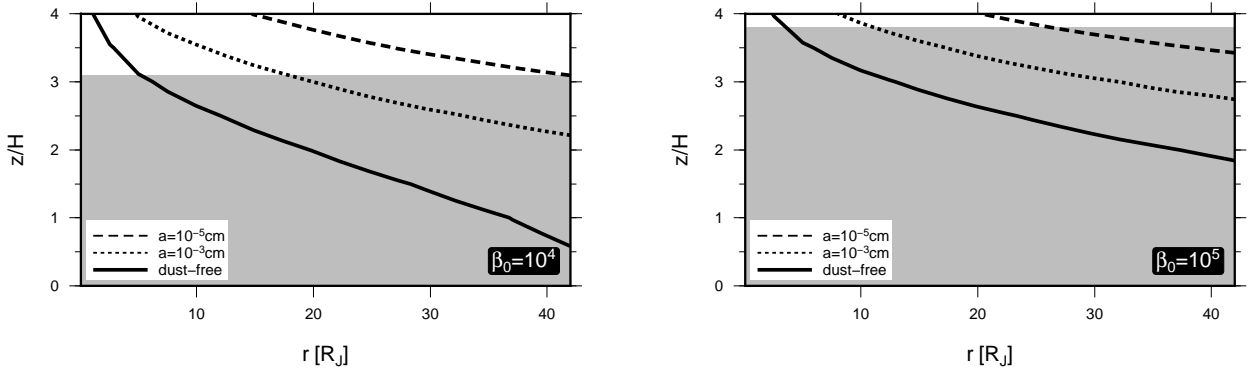


Figure 4. Same as Figure 3 but for the case of $\epsilon = 10^{-3}$. The radius of dust grains, a , used in these calculations is indicated in the figure.

Fig. 3 shows the results for the case of $\alpha = 0.05$, $\epsilon = 1$, and $f_{\text{dg}} = 0$. The region above the solid line $\Lambda = 1$ and inside the gray shaded area ($\beta_z > 8\pi^2$) is unstable to MRI as dictated by the conditions discussed in Section 2.1. The hatched region illustrates $\beta_z > 2000$, the criterion for turbulence to be well developed (refer to Equation 6). Thus, a region of well-developed MRI turbulence is above $\Lambda = 1$ and within the hatched region. For the parameters of Fig. 3, there is no region that has well-developed MRI turbulence. This means that under these settings, the MRI cannot generate the accretion stress, $\alpha = 0.05$, which we have assumed in the calculations of surface density. A calculation with smaller α results in a smaller region with $\Lambda > 1$ because the surface density is larger and the ionization degree is lower. Consequently, we cannot find a self-consistent solution for Σ and α when $\epsilon = 1$.

The results for $\epsilon = 10^{-3}$ are shown in Fig. 4, which corresponds to the case of gap opening or global disk dispersal. Without dust grains, active layers with well-developed turbulence appear at large radii, but with dust grains, such layers do not exist in satellite-forming regions. Fig. 5 shows the results for $\epsilon = 10^{-5}$. The MRI-active layers become thicker but the situation does not change dramatically. It is difficult to sustain well-developed MRI turbulence in circumplanetary disks with dust grains, especially in areas experiencing gas infall.

When the surface density is smaller, the ionization degree is larger and the line $\Lambda = 1$ is lower. We estimate the minimum surface density needed to form satellites to find the lower limit of the line $\Lambda = 1$. The timescale to form a

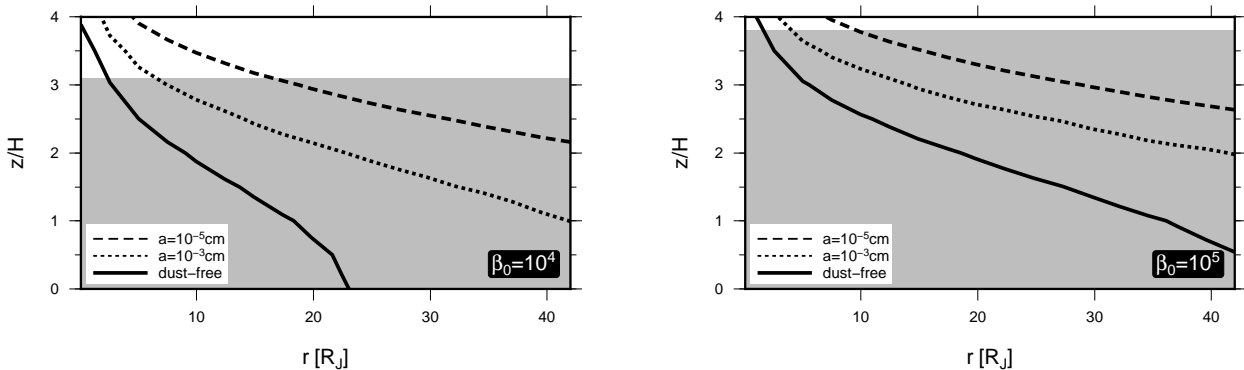


Figure 5. Same as Fig. 4 but for the case of $\epsilon = 10^{-5}$.

satellite of radius R_s and density ρ_s orbiting at r is

$$\begin{aligned} \tau_s &\approx \frac{1}{\Omega} \frac{\rho_s R_s}{\Sigma_{\text{sol}} F_g} \\ &\sim 8 \text{yr} \left(\frac{R_s}{2500 \text{ km}} \right) \left(\frac{\rho_s}{2 \text{ g cm}^{-3}} \right) \left(\frac{F_g}{100} \right)^{-1} \\ &\quad \times \left(\frac{\Sigma_{\text{sol}}}{3 \times 10^3 \text{ g cm}^{-2}} \right)^{-1} \left(\frac{r}{15 R_J} \right)^{3/2}, \end{aligned} \quad (26)$$

where Σ_{sol} is the surface density of solids and $F_g \equiv 1 + (v_{\text{esc}}/v_\infty)^2$ is the gravitational focusing factor for colliding objects with relative velocity at infinity v_∞ and mutual escape velocity v_{esc} (Lissauer & Stewart 1993; Ward 1996; Canup & Ward 2002). To form a satellite whose radius, density, and orbit are similar to Ganymede's within the lifetime of the disk, $\tau_s \sim 10^7$ yr, the required surface density of solids is

$$\Sigma_{\text{sol}} \sim 10^{-3} \text{ g cm}^{-2} \left(\frac{r}{15 R_J} \right)^{3/2} \left(\frac{R_s}{2500 \text{ km}} \right) \left(\frac{\rho_s}{2 \text{ g cm}^{-3}} \right) \left(\frac{F_g}{100} \right)^{-1}. \quad (27)$$

The value of F_g depends on the size of the proto-satellite. Since we want to know the minimum value of Σ_{sol} , we choose the maximum value of the gravitational focusing factor, $F_g \sim 100$, when $v_\infty \simeq (M_s/3M_p)^{1/3} v_K$ (v_K is the Keplerian velocity around the planet at the proto-satellite orbit). If we assume the dust-to-gas mass ratio does not depend on the height and take $f_{\text{dg}} = 10^{-2}$, the surface density of gas should be larger than $\Sigma \sim 0.1 \text{ g cm}^{-2}$. According to this estimation, and Fig. 2, it seems quite difficult to form satellites with $\epsilon = 10^{-5}$ or smaller. Therefore, we do not consider even smaller infall rates.

Next, we investigate the surface density at each radius that can sustain well-developed MRI turbulence. The results are summarized in Fig. 6. The surface densities which can sustain well-developed turbulence for $z > 2H$, $z > 0.5H$, and for the entire height at each radius are shown. The mid-plane plasma beta considered here is $\beta_0 = 10^5$. If we choose larger β_0 , the line $\Lambda = 1$ shifts higher which means the MRI-active region becomes smaller. On the other hand, if we choose smaller β_0 , the region with $\beta_z > 2000$ is smaller, and having large MRI-active regions becomes difficult.

5. DISCUSSION

We find that when accounting for cosmic rays, X-rays, and radionuclides, circumplanetary disks are not likely to sustain well-developed MRI turbulence. In contrast to protoplanetary disks, the volume ratio of MRI-active regions to dead zones for circumplanetary disks is very small. This is because the typical length scale of circumplanetary disks is smaller by several orders of magnitude than that of protoplanetary disks. This makes the timescale of magnetic diffusion smaller. According to Equation (1), even if v_{Az} and η are the same, the Elsasser number tends to be smaller in circumplanetary disks. For example, the typical ionization degree at 5AU in a protoplanetary disk and that at $15R_J$ in a circumplanetary disk are both $\sim 10^{-10}$, but the Keplerian frequency of a protoplanetary disk at 5AU is $\sim 10^{-8} \text{ s}^{-1}$ and that of a circumplanetary disk at $15R_J$ is $\sim 10^{-5} \text{ s}^{-1}$. Therefore, it is very difficult for MRI turbulence to be well developed in circumplanetary disks unless the surface density is very small, as we show in Fig. 6.

Recently, Turner, Lee, & Sano (2014) have investigated the possibility of the MRI in various models of circumplanetary disks from the literature. They choose the mid-plane value of plasma beta to be 10^3 . Their condition to have the MRI is that the magnetic pressure is smaller than the gas pressure, which is satisfied below 3.7 scale heights. They concluded that there are active layers at the disk surface. Our results are consistent with theirs when we choose the condition that $\beta_z > 8\pi^2$ to sustain the MRI. For example, Figure 3 of Turner et al. (2014) and Fig. 3 of this paper show similar models of surface density, and both have surface active layers. Note that even if the MRI can be sustained

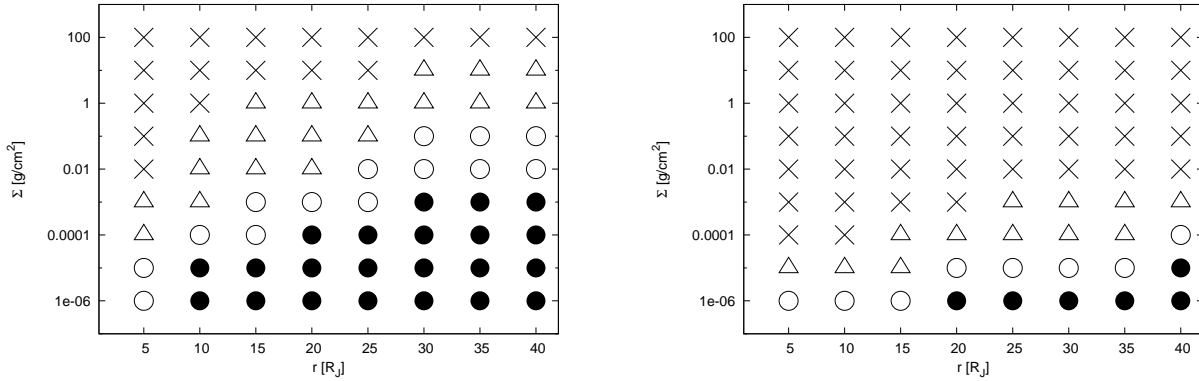


Figure 6. Surface densities of MRI-active at each radius. ● represents the surface densities at the given radius which have well-developed MRI turbulence at the entire height, ○ represents that at only above $0.5H$, and △ represents that at only above $2H$. Since we choose $\beta_0 = 10^5$, $\beta_z < 2000$ above $2.8H$ and well-developed turbulence cannot be sustained in such region. We plot × for the surface densities in which we cannot find regions of $\Lambda > 1$ below $2.5H$. The left panel is the result of a dust free calculation and the right panel is that of a case with dust grains of $a = 0.1\mu\text{m}$. With dust grains, the MRI-active region is smaller because of the lower ionization degree.

at the disk surface, it does not necessarily mean that there is well-developed turbulence. When MRI turbulence is well developed, the magnetically dominated atmosphere encroaches on a lower altitude and a region of well-developed turbulence becomes smaller (Okuzumi & Ormel 2013). The main difference between Turner et al. (2014) and our work is that we consider the criterion for turbulence to be well developed as well as that of just having MRI.

If there are no other mechanisms to give rise to viscosity and disks are not massive, the gas piles up in circumplanetary disks until the disks become massive enough to be gravitationally unstable. It is possible to promote gas accretion by GI, but it may not reduce the disk surface density much below the critical value for GI. Therefore the surface density is expected to remain large.

As we mentioned, if only GI can generate gas accretion, a massive and static disk will remain even after infall from the protoplanetary disk terminates. This suggests that the lifetime of circumplanetary disks may be longer than that of protoplanetary disks. Thus, perhaps we are more likely to be able to observe circumplanetary disks than previously thought (e.g., Mamajek et al. 2012), and satellite formation may occur over a long timescale. On the other hand, it remains important to consider other mechanisms for angular momentum transport. A possible mechanism is spiral density waves caused by a non-axisymmetric potential (e.g., Machida et al. 2010; Martin & Lubow 2011b; Rivier et al. 2012; Szulagyi et al. 2014), but this must be investigated in more detail.

If there is viscous heating in such a massive disk, it will easily heat up, and thermal ionization may drive the MRI (Lubow & Martin 2012). Even if GI can drive turbulence, it does not necessarily mean the turbulence can generate heat in situ. The question of where the energy dissipates remains open (Balbus & Papaloizou 1999; Goodman & Rafikov 2001; Muto et al. 2010). We should be careful in treating the heating by gravitational turbulence. Further study of energy dissipation by GI is necessary.

If thermal ionization triggers the MRI, disks would be less massive because of a high accretion rate. Suppose that if at each annulus of a disk, gravitational energy is converted into thermal energy and radiates as a black body from the disk surface, the effective temperature is

$$T_{\text{eff}} = \left(\frac{3GM_p\dot{M}}{8\pi\sigma_{\text{SB}}r^3} \right)^{1/4}, \quad (28)$$

where M_p is the planet mass, \dot{M} is the mass accretion rate, and σ_{SB} is the Stefan-Boltzmann constant. We can estimate the mid-plane temperature, T_c , from the approximation $T_c \simeq \tau^{1/4}T_{\text{eff}}$ ($\tau \gg 1$), where τ is optical depth, given by $\tau \sim \kappa\Sigma$ where κ is opacity. Here we use $\dot{M} = 3\pi\nu\Sigma$. Then, the mid-plane temperature can be written as

$$T_c = 1.0 \times 10^3 \left(\frac{\kappa}{5 \text{ cm}^2 \text{ g}^{-1}} \right)^{1/5} \left(\frac{\alpha}{10^{-2}} \right)^{-1/5} \left(\frac{M_p}{M_J} \right)^{3/10} \\ \times \left(\frac{\dot{M}}{3.1 \times 10^{-7} M_J \text{ yr}^{-1}} \right)^{2/5} \left(\frac{r}{10R_J} \right)^{-9/10} \text{ K}, \quad (29)$$

where M_J is the Jupiter mass. When the mid-plane temperature exceeds about 1000K, gas in the disk will be sufficiently ionized to have the MRI. The inner disk may be hot enough to have thermal ionization especially during the early phases of gas giant formation; however, the outer disk seems to remain cool. More detailed calculations of the mid-plane temperature of circumplanetary disks have been done by Keith & Wardle (2014).

Another possibly important mechanism for satellite formation is the capture of planetesimals when they cross circumplanetary disks (Fujita et al. 2013) (see Estrada & Mosqueira 2006, for the gas-poor case). Since our results

suggest a large surface density, capture is expected to be effective. Non-axisymmetry in the density structure caused by these proto-satellites may play a role in angular momentum transport and it may be interesting to analyze that effect.

6. SUMMARY

We estimated the size of regions that can sustain magnetic turbulence in circumplanetary disks. We calculated the ionization degree in disks accounting for galactic cosmic rays, X-rays from the host star of the surrounding protoplanetary disk, and the decay of short-lived radionuclides as ionization sources, and evaluated the MRI activity. We adopted the α model and solved the diffusion equation of a disk with infalling mass flux from a protoplanetary disk, obtained by Tanigawa et al. (2012). Even by varying parameters such as gas infall rate, magnetic field, dust-to-gas mass ratio, and radius of dust grains over a wide range, it was difficult to find a sufficiently sized MRI-active region that can sustain well-developed turbulence, a region where both the Elsasser number is larger than unity and the magnetic pressure is sufficiently smaller than the gas pressure. We found that the surface density that can sustain well-developed MRI turbulence is $\Sigma \sim 0.001\text{--}0.01 \text{ g cm}^{-2}$, even without dust grains, for a typical satellite-forming region. Note that we have performed the calculations for a very optimistic set of assumptions for activation of the MRI. If metals are frozen out onto dust grains or cosmic rays are shielded by stellar activities, situations become much severer to sustain MRI.

If there are MRI-active regions, we can estimate the accretion stress with the empirical formula of Okuzumi & Hirose (2011); Okuzumi & Ormel (2013). However, we find that the MRI is unlikely to be well developed in circumplanetary disks with cosmic rays, X-rays, and radionuclides; even if the MRI can be initiated, the active turbulence cannot be sustained. As long as the MRI is the only mechanism of gas accretion in less massive disks, our results suggest that disk surface density increases until it becomes gravitationally unstable. If this is the case, the picture of satellite formation should be changed. In order to examine this suggestion, we have to investigate other possible mechanisms such as spiral density waves, baroclinic instability, or global magnetic braking.

In this paper, we have used the analysis of Tanigawa et al. (2012) for the formation phases of circumplanetary disks. However, the long-term evolution of the gas infall rate from a protoplanetary disk to a circumplanetary disk is not yet well understood. To investigate this further, it is necessary to know the evolution of protoplanetary disks, such as the gap opening timescale and its effect on density structure. We need to study how a change in the density of protoplanetary disks affects the infall rate onto circumplanetary disks.

We thank Sanemichi Z. Takahashi and Hiroshi Kobayashi for fruitful discussions. We are grateful to the anonymous referees for useful comments that improved our manuscript. We appreciate Jennifer M. Stone's help in improving our English, and Takeru K. Suzuki's continuous encouragement. This work was supported by JSPS KAKENHI Grant Numbers 24-4770, and 25887023, and by MEXT KAKENHI Grant Numbers 23740326, 24103503, 23244027, and 23103005.

REFERENCES

- Ayliffe, B. A., & Bate, M. R. 2009a, *MNRAS*, 397, 657
 —. 2009b, *MNRAS*, 393, 49
 Balbus, S. A., & Hawley, J. F. 1991, *ApJ*, 376, 214
 Balbus, S. A., & Papaloizou, J. C. B. 1999, *ApJ*, 521, 650
 Blaes, O. M., & Balbus, S. A. 1994, *ApJ*, 421, 163
 Canup, R. M., & Ward, W. R. 2002, *AJ*, 124, 3404
 —. 2006, *Nature*, 441, 834
 —. 2009, *Europa*, ed. R. T. Pappalardo, W. B. McKinnon, & K. K. Khurana, 59
 Cleves, L. I., Adams, F. C., & Bergin, E. A. 2013, *ApJ*, 772, 5
 Crida, A., & Charnoz, S. 2012, *Science*, 338, 1196
 Ercolano, B., & Glassgold, A. E. 2013, *MNRAS*
 Estrada, P. R., & Mosqueira, I. 2006, *Icarus*, 181, 486
 Estrada, P. R., Mosqueira, I., Lissauer, J. J., D'Angelo, G., & Cruikshank, D. P. 2009, *Europa*, ed. R. T. Pappalardo, W. B. McKinnon, & K. K. Khurana, 27
 Fujii, Y. I., Okuzumi, S., & Inutsuka, S. 2011, *ApJ*, 743, 53
 Fujita, T., Ohtsuki, K., Tanigawa, T., & Suetsugu, R. 2013, *AJ*, 146, 140
 Gammie, C. F. 1996, *ApJ*, 457, 355
 Goodman, J., & Rafikov, R. R. 2001, *ApJ*, 552, 793
 Gressel, O., Nelson, R. P., & Turner, N. J. 2012, *MNRAS*, 422, 1140
 Gressel, O., Nelson, R. P., Turner, N. J., & Ziegler, U. 2013, *ApJ*, 779, 59
 Hayashi, C. 1981, *Progress of Theoretical Physics Supplement*, 70, 35
 Igea, J., & Glassgold, A. E. 1999, *ApJ*, 518, 848
 Ilgner, M., & Nelson, R. P. 2006, *A&A*, 445, 205
 Keith, S. L., & Wardle, M. 2014, *MNRAS*, 440, 89
 Klahr, H., & Kley, W. 2006, *A&A*, 445, 747
 Lissauer, J. J., & Stewart, G. R. 1993, in *Protostars and Planets III*, ed. E. H. Levy & J. I. Lunine, 1061–1088
 Lubow, S. H., & Martin, R. G. 2012, *ApJ*, 749, L37
 Lubow, S. H., Seibert, M., & Artymowicz, P. 1999, *ApJ*, 526, 1001
 Lunine, J. I., & Stevenson, D. J. 1982, *Icarus*, 52, 14
 Machida, M. N., Inutsuka, S., & Matsumoto, T. 2006, *ApJ*, 649, L129

- Machida, M. N., Kokubo, E., Inutsuka, S., & Matsumoto, T. 2010, MNRAS, 405, 1227
Machida, M. N., Kokubo, E., Inutsuka, S., & Matsumoto, T. 2008, ApJ, 685, 1220
Mamajek, E. E., Quillen, A. C., Pecauc, M. J., et al. 2012, AJ, 143, 72
Martin, R. G., & Lubow, S. H. 2011a, ApJ, 740, L6
—, 2011b, MNRAS, 413, 1447
Mosqueira, I., & Estrada, P. R. 2003a, Icarus, 163, 198
—, 2003b, Icarus, 163, 232
Muto, T., Suzuki, T. K., & Inutsuka, S. 2010, ApJ, 724, 448
Ogihara, M., & Ida, S. 2012, ApJ, 753, 60
Okuzumi, S. 2009, ApJ, 698, 1122
Okuzumi, S., & Hirose, S. 2011, ApJ, 742, 65
Okuzumi, S., & Ormel, C. W. 2013, ApJ, 771, 43
Oppenheimer, M., & Dalgarno, A. 1974, ApJ, 192, 29
Rivier, G., Crida, A., Morbidelli, A., & Brouet, Y. 2012, A&A, 548, A116
Sano, T., & Miyama, S. M. 1999, ApJ, 515, 776
Sano, T., Miyama, S. M., Umebayashi, T., & Nakano, T. 2000, ApJ, 543, 486
Sasaki, T., Stewart, G. R., & Ida, S. 2010, ApJ, 714, 1052
Shakura, N. I., & Sunyaev, R. A. 1973, A&A, 24, 337
Szulagyi, J., Morbidelli, A., Crida, A., & Masset, F. 2014, ApJ, 782, 65
Tanigawa, T., Ohtsuki, K., & Machida, M. N. 2012, ApJ, 747, 47
Tanigawa, T., & Watanabe, S. 2002, ApJ, 580, 506
Turner, N. J., Lee, M. H., & Sano, T. 2014, ApJ, 783, 14
Turner, N. J., & Sano, T. 2008, ApJ, 679, L131
Umebayashi, T., & Nakano, T. 1981, PASJ, 33, 617
—, 2009, ApJ, 690, 69
Ward, W. R. 1996, in *Astronomical Society of the Pacific Conference Series, Vol. 107, Completing the Inventory of the Solar System*, ed. T. Rettig & J. M. Hahn, 337–361